Sulfamate synthesis via aqueous electrocatalytic N–S coupling through interfacial microenvironment optimization

Zhihui Yao,[a] *Daisong Chen,*[b] *Jin Shang,*[b] *Tian Zeng,*[c,*] *and Edmund C. M. Tse*[a,*]

[a] Department of Chemistry, HKU-CAS Joint Laboratory on New Materials

The University of Hong Kong

Hong Kong SAR, China

[b] School of Energy and Environment

City University of Hong Kong

Hong Kong SAR, China

[c] School of Chemical Engineering

Northwest University

Xi'an, Shanxi, China

[*] E-mail: TZ u3006411@connect.hku.hk; ECMT ecmtse@hku.hk

Note S1. Chemical reagents

Carbon paper (0, 20%, 40%, and 60% PTFE, TPG-H-060) were purchased from Toray, Japan. Sodium sulfide ($Na_2S·9H_2O$, ≥ 98%), Lithium hydroxide (LiOH, anhydrous), cyclohexylamine ($C_6H_{11}NH_2$, ≥ 99.0%), and cyclamic acid ($C_6H_{11}NH_2SO_3H$, ≥ 98.0%) were purchased from Aladdin Industrial Co., Ltd, Shanghai, China. Ammonia (NH_3 in water, 32%) was purchased from VWR BDH chemicals, France. Potassium hydroxide (KOH, AR) and sodium hydroxide (NaOH, AR) were purchased from Dieckmann HK Chemical Industry Co., Ltd, Hong Kong SAR, China. Sulfamic acid (H_3NO_3S, 99.5%) and Cesium hydroxide monohydrate (CsOH, 99.5%) were purchased from Macklin Biochemical Technology Co., Ltd, Shandong, China. Sodium sulfate (Na_2SO_4, ≥ 99.0%) was purchased from Sigma Aldrich Chemie GmbH, Steinheim, Germany.

Note S2. Characterizations

X-ray diffraction (XRD) patterns were collected from an X-ray powder diffractometer (Bruker D8 Advance) with Cu Kα radiation at 40 kV and 40 mA and a LynxEye detector. The angle ranged from 10° to 80°, step size was 0.02, and time per step was 2 s. Surface morphologies of CPs were characterized using a scanning electron microscope (SEM; Leo 1530 FEG). Energy-dispersive X-ray spectroscopy (EDS) images were obtained using an X-Max 50 EDS detector. Chemical compositions and valence states of elements were determined by X-ray photoelectron spectroscopy (XPS; Thermo Scientific Escalab QXi), and the binding energies were corrected through C 1s peak (284.8 eV). Thermogravimetric analysis (TGA) was conducted on a METTLER TOLEDO thermogravimetric analyzer in dry nitrogen flow. The CPs were heated from 25 ℃ to 800 ℃ with a ramping rate of 6 ℃ min^{-1}. N_2 sorption isotherms were measured on a BSD adsorption analyzer (BSD-660 MG).

^1H nuclear magnetic resonance (^1H-NMR) was used for structure analysis. Electrolyte after reaction was firstly adjusted to acidic using H_2SO_4, stirring for H_2S, SO_2 removal and S_0 precipitation. Then, $Ba(OH)_2$ was added to precipitate sulfate ions.

After filtration, H-type ion exchange resin was added to exchange the cations in solution. Finally, N-S coupling products were obtained through crystallization at 60°. For ^{1}H NMR measurement, sulfamic acid and N-S coupling products were dissolved in 600 uL deuterated dimethyl sulfoxide (DMSO-d6). On the NMR spectra, the characteristic signals for $–NH_2$ was three identically spaced peaks.

Note S3. Electrochemical equations

FE for a specific product was calculated based on the Eq. S1:

$$\mathrm{FE}(\%) = \frac{n \times c \times V \times \mathrm{F}}{Q} \times 100 \quad \text{(Eq. S1)}$$

Yield rate was calculated using Eq. S2:

$$\text{Yield Rate } (\mathrm{mmol \cdot h^{-1} \cdot cm^{-2}}) = \frac{c \times V}{t \times A} \quad \text{(Eq. S2)}$$

In the above equations, n was the number of electrons transferred during nitrate reduction to form products (n = 8 for sulfamate and sulfate); c was the concentration of the products (mol L^{-1}); V was the volume of cathodic electrolyte solution (L); F was the Faraday constant (F = 96485 C mol^{-1}); Q was the total amount of charge consumed (C); t was the reaction time (h); A was the reaction area.

Note S4. Calculation methods

General computational details and thermodynamic corrections

All density functional theory (DFT) calculations were performed using the Gaussian 16 software package. Geometry optimizations and vibrational frequency calculations were conducted using the B3LYP functional supplemented with Grimme's D3 empirical dispersion correction with Becke-Johnson damping (GD3BJ) at the 6-31+G(d) basis set level.[1-3] To obtain more accurate electronic energies, single-point energy calculations were subsequently performed using the 6-311+G(d,p) basis set based on the optimized geometries. After geometry optimization, the Gibbs free energy of the molecules in solution (G_{sol}) was evaluated according to the thermodynamic cycle (Eq. S3)

$$G_{sol} = G_{gas} + \Delta G_{solv} + \Delta G^{1\mathrm{atm}\rightarrow 1\mathrm{M}} \quad \text{(Eq. S3)}$$

where G_{gas} is the gas-phase free energy, ΔG_{solv} is the solvation free energy, and $\Delta G^{1atm \rightarrow 1M}$ represents the standard state conversion correction from 1 atm to 1 M concentration (1.89 kcal mol^{-1} at 298.15 K).

Modeling of bulk and interfacial systems

To systematically investigate the reaction energetics under various hydrophobic microenvironments, the implicit Solvation Model based on Density (SMD) was employed. Importantly, to realistically simulate the local solvation environment and the intricate hydrogen-bonding network in the bulk solution, a micro-solvation cluster approach was adopted, wherein explicit water molecules (e.g., $3H_2O$) were introduced to surround the anionic core. The specific degree of interfacial hydrophobicity was simulated by continuously downscaling the dielectric constant (ε) of the solvent from bulk water ($\varepsilon = 78$) to a series of lower values (70, 60, 50, 40, 30, 20, and 10).

To simulate the interfacial reactions under alkaline conditions, a hydroxyl-functionalized coronene cluster (denoted as $C_{24}H_{12}$–OH) was used to represent the active carbon cloth electrode surface. The adsorption process proceeds via a deprotonation mechanism, wherein the attacking SO_3^{2-} intermediate deprotonates the surface hydroxyl group to form a stable surface C–O–S linkage. During the geometry optimizations, a selective partial relaxation strategy was applied to balance the structural rigidity of the bulk carbon lattice with the required local flexibility at the active site. Specifically, the peripheral carbon and hydrogen atoms of the coronene substrate were constrained to their original positions. Conversely, the surface-active oxygen atom, the specific anchor carbon atom bonded to it, the three directly adjacent carbon atoms, and the adsorbate were fully relaxed. This treatment accommodates necessary local structural deformations and relieves steric strain during bulky bond formation, while preventing artificial global curling of the finite cluster. To accurately account for the aqueous alkaline electrolyte environment, the implicit SMD solvation model was utilized using a dielectric constant of $\varepsilon = 78$ to represent bulk water. Geometry optimizations and single-point energies on the surface were performed using

the identical B3LYP-GD3BJ/6-31+G(d) and 6-311+G(d,p) dual-basis-set strategy as the bulk phase.

Electrochemical thermodynamics and potential corrections

The computational hydrogen electrode (CHE) model was employed to calculate the electrochemical free energies of the reaction intermediates. Initially, the reference potential was set to the standard hydrogen electrode (SHE). The pH effect on the chemical potential of protons was explicitly considered by adding a concentration correction term of Eq. S4.

$-k_B \ln(10) \times \mathrm{pH}$ (equivalent to $-0.0592 \times \mathrm{pH}$ in eV at 298.15 K) (Eq. S4)

Furthermore, to enable a direct comparison with experimental cyclic voltammograms, the calculated potentials were referenced to the reversible hydrogen electrode (RHE). Consequently, the applied electrode potential (U) versus SHE was converted using the Nernst relation (Eq. S5).

$$U_{\mathrm{SHE}} = U_{\mathrm{RHE}} - 0.0592 \times \mathrm{pH} \quad \text{(Eq. S5)}$$

For instance, the free energy shift for an electrochemical step can be generalized by incorporating both corrections (Eq. S6)

$$\Delta G(U, \mathrm{pH}) = -0.0592 \times \mathrm{pH} - ne(U_{\mathrm{RHE}} - 0.0592 \times \mathrm{pH}) \quad \text{(Eq. S6)}$$

where n represents the number of transferred electrons.

Supplementary Figures

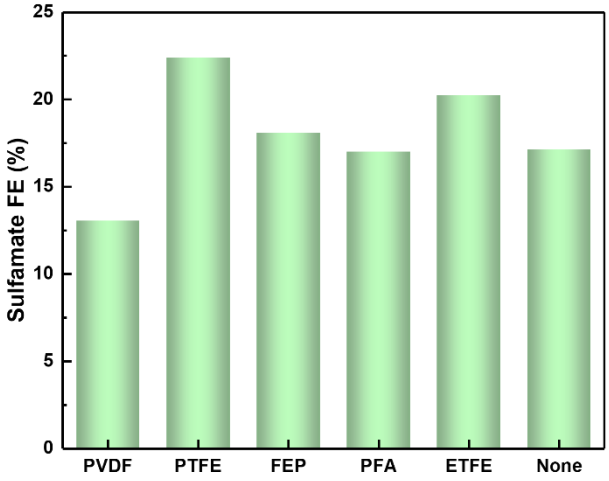

Fig. S1. Sulfamate FEs of CPs modified with fluorinated polymers in electrolytes containing 0.1 M KOH, 0.5 M NH_3 and 10 mM S^{2-} at 2.5 V vs. RHE.

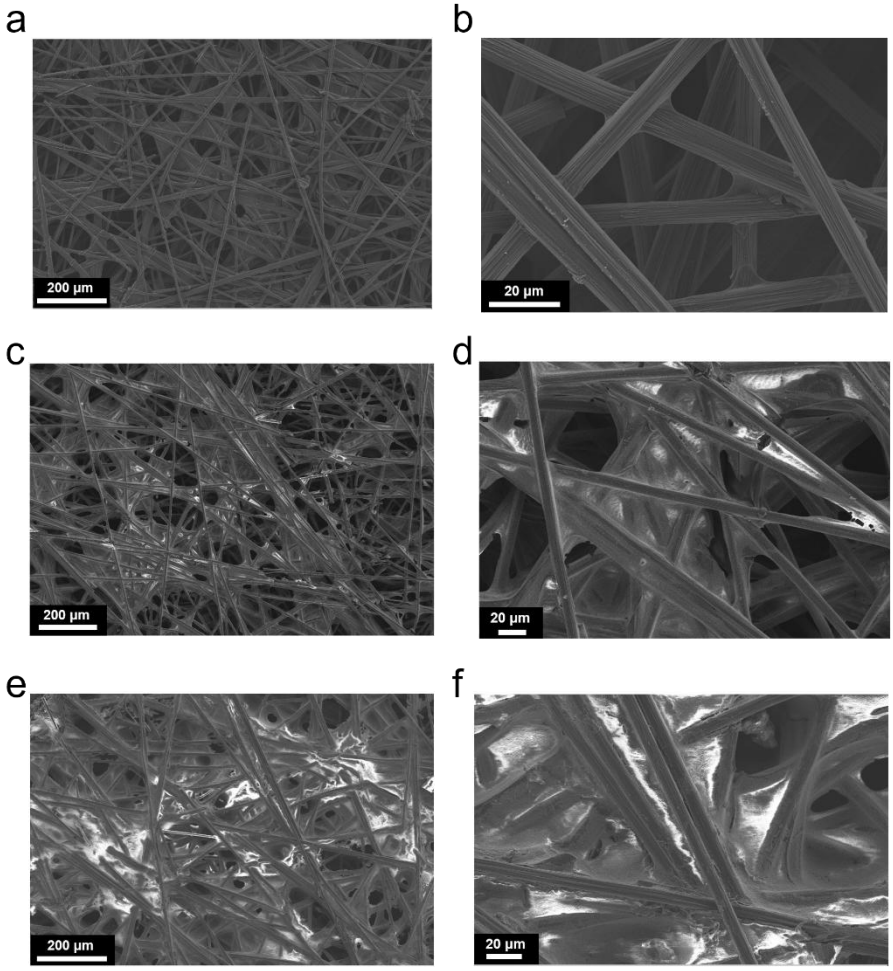

Fig. S2. SEM images of a, b) CP, c, d) 20% PTFE CP, and e, f) 60% PTFE CP.

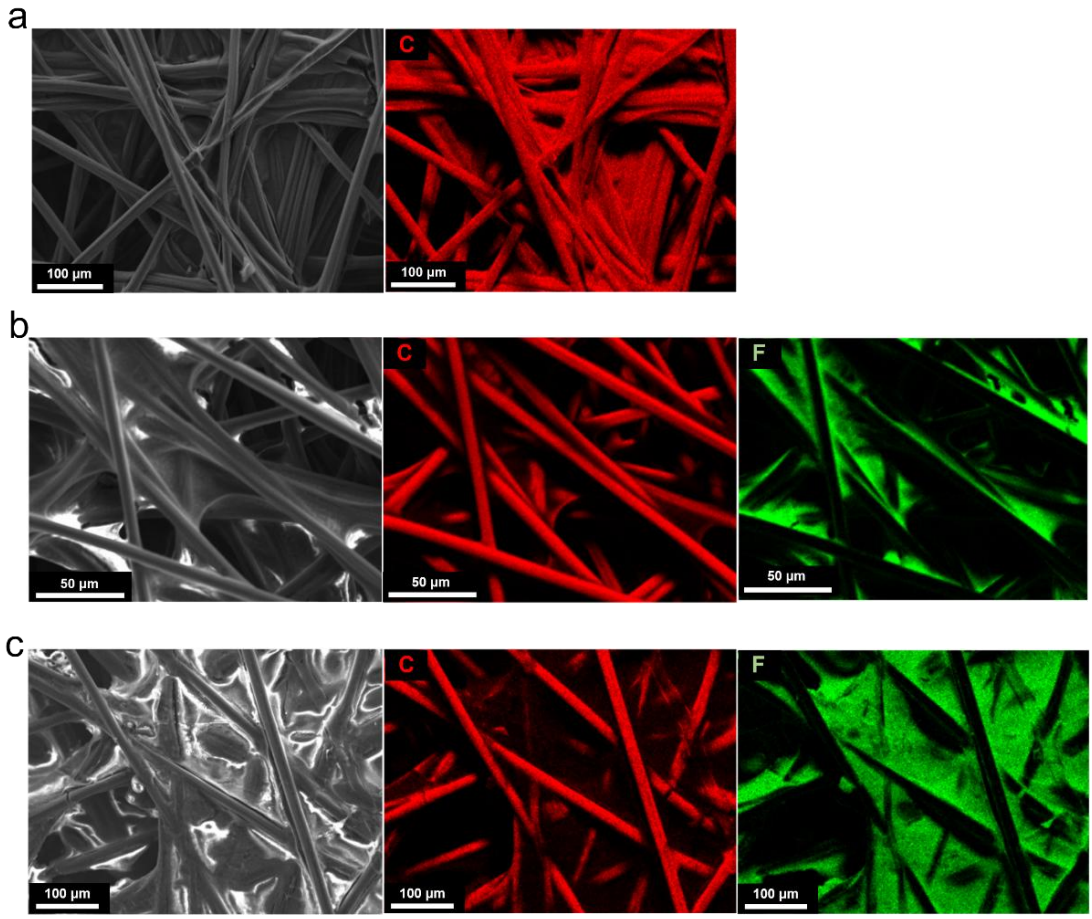

Fig. S3. EDS mappings of a) CP, b) 20% PTFE CP, and c) 60% PTFE CP.

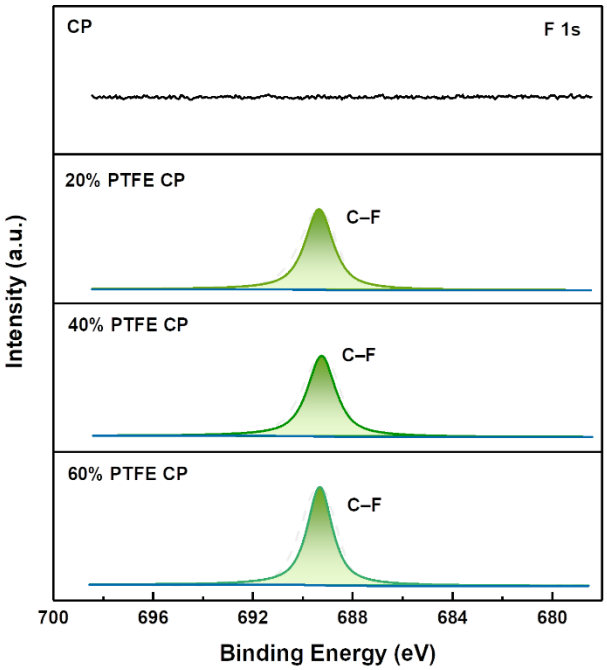

Fig. S4. High-resolution F 1s spectra of designed CPs.

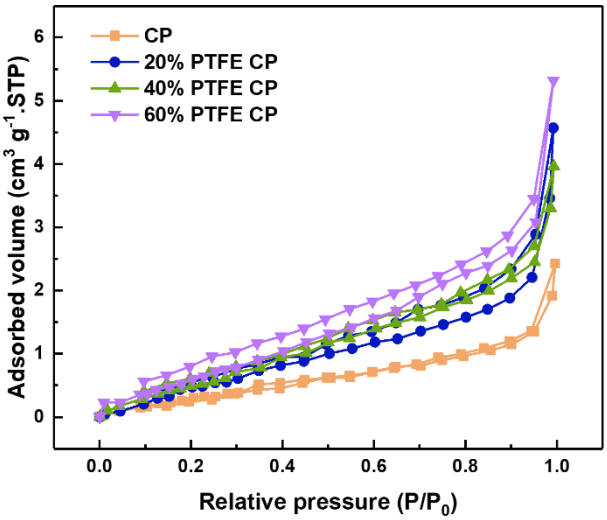

Fig. S5. Nitrogen adsorption and desorption isotherms for designed CPs.

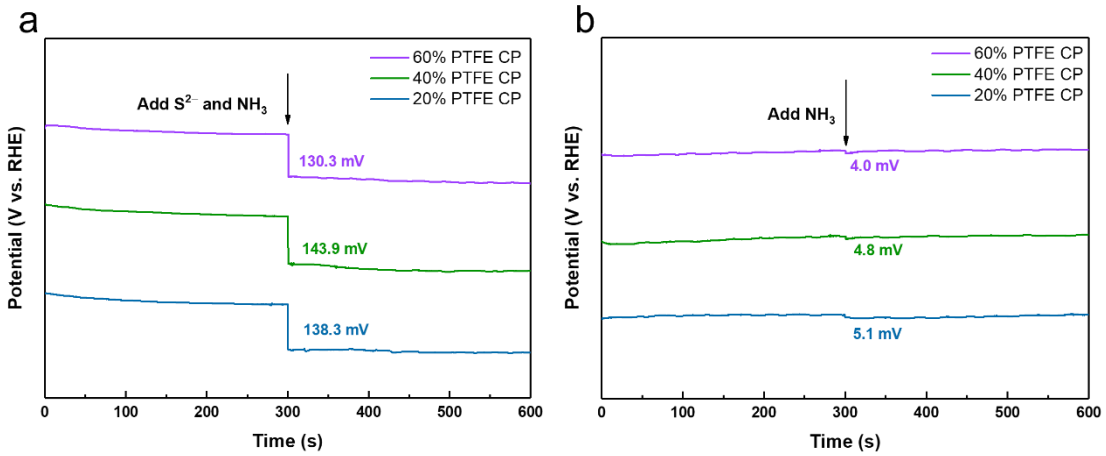

Fig. S6. OCP response of a) S^{2-} and NH_3, and b) NH_3 on designed CPs.

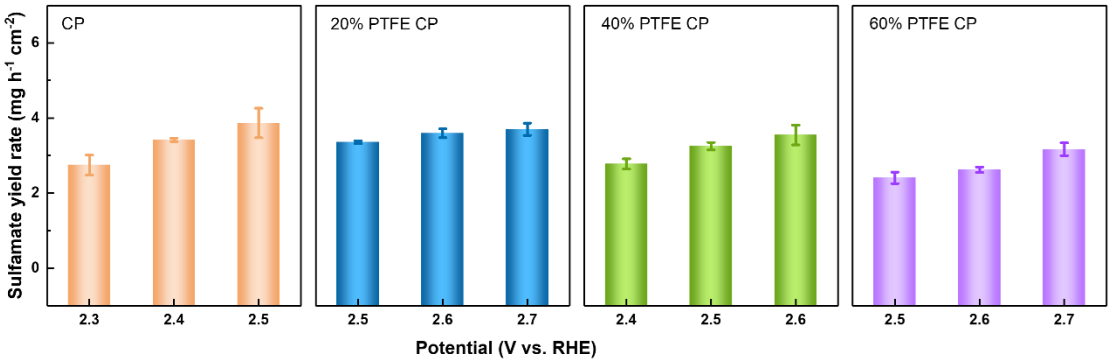

Fig. S7. Sulfamate yield rate of designed CPs in electrolyte containing 0.1 M KOH, 0.5 M NH_3 and 10 mM S^{2-}.

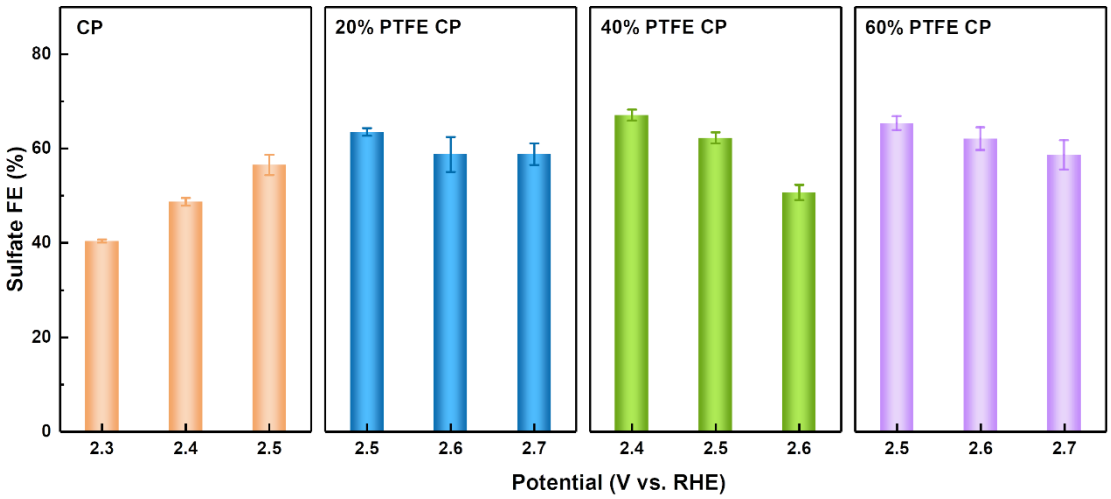

Fig. S8. Sulfate FEs for designed CPs in electrolyte containing 0.1 M KOH, 0.5 M NH_3 and 10 mM S^{2-}.

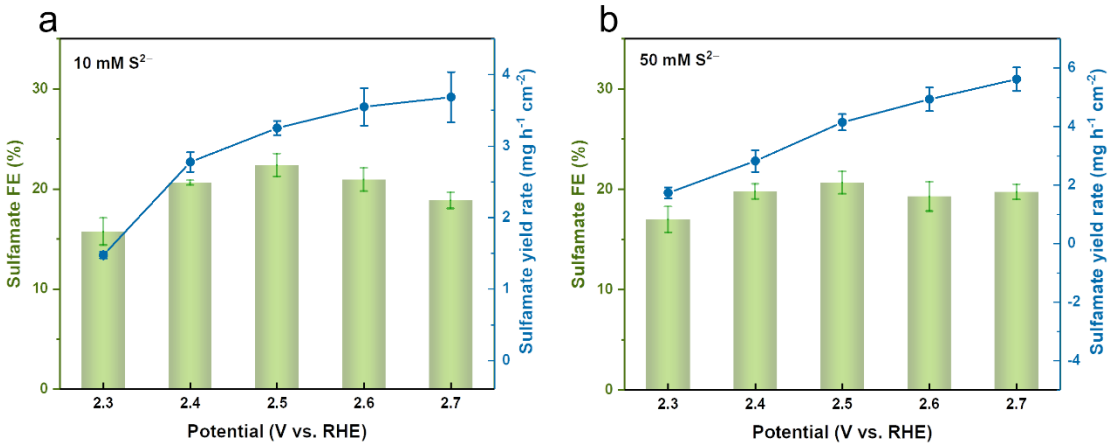

Fig. S9. Sulfamate FEs and yield rates in 0.1 M KOH and 0.5 M NH_3 with a) 10 mM S^{2-}, and b) 50 mM S^{2-}.

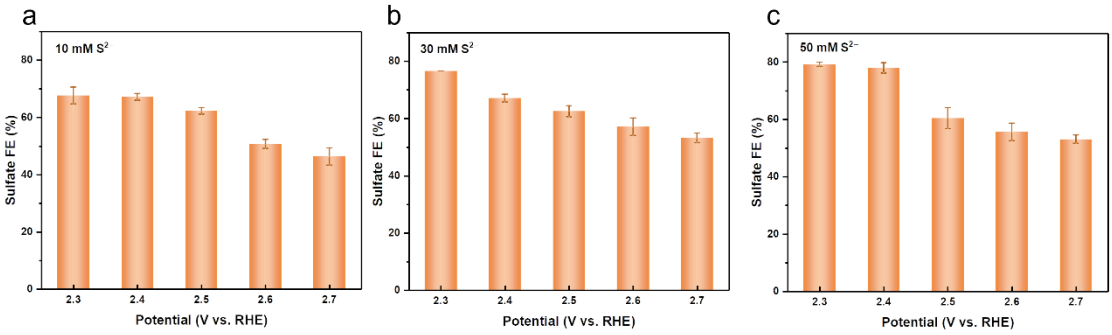

Fig. S10. Sulfate FEs in 0.1 M KOH and 0.5 M NH_3 with a) 10 mM S^{2-}, b) 30 mM S^{2-}, and c) 50 mM S^{2-}.

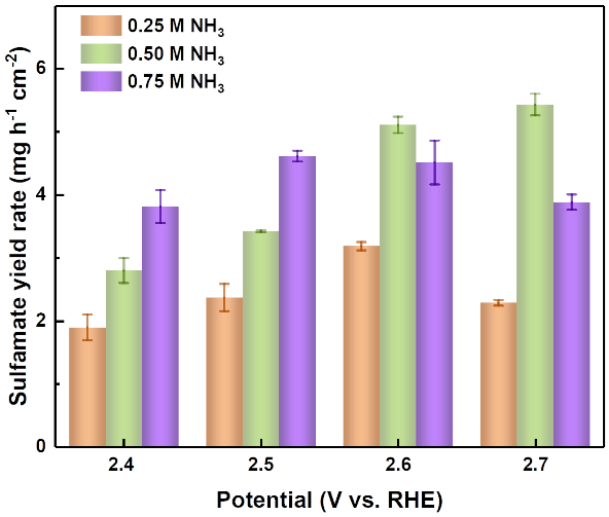

Fig. S11. Sulfate FEs in 0.1 M KOH and 30 mM S^{2-} with designed NH_3 concentrations.

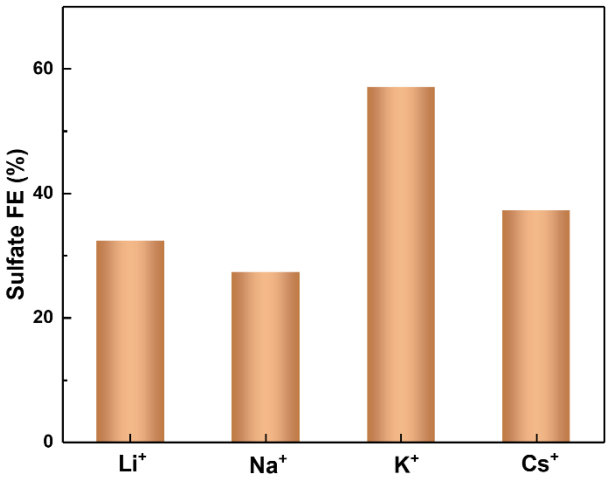

Fig. S12. Sulfate FEs in electrolytes with designed cations (Li^+, Na^+, K^+, and Cs^+).

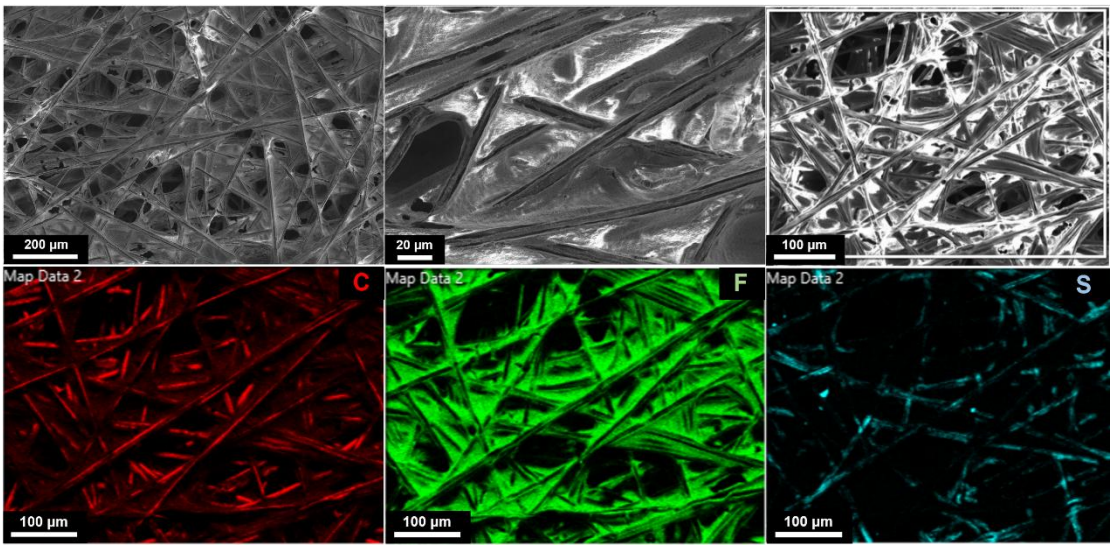

Fig. S13. SEM images and EDS mappings of 40% PTFE CP after long-term reaction.

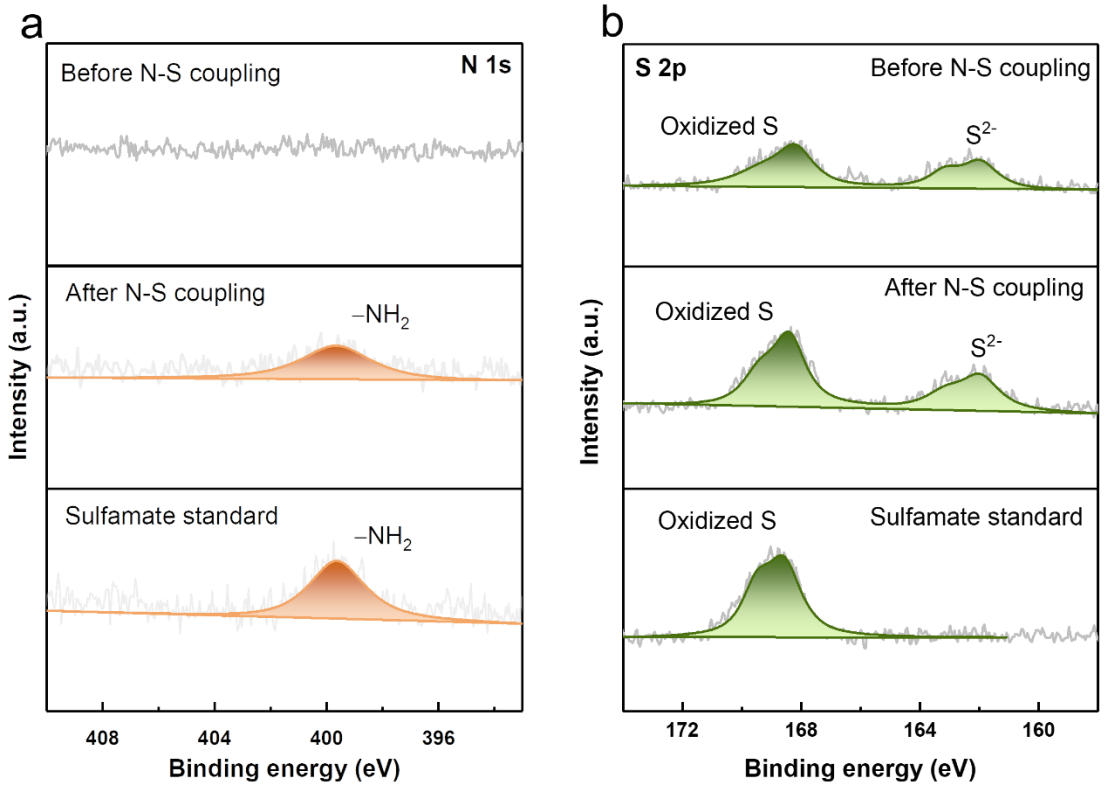

Fig. S14. a) high-resolution N 1s spectra, and b) high-resolution S 2p spectra of sulfamate standard solution and electrolytes before and after N–S coupling reaction on CPs.

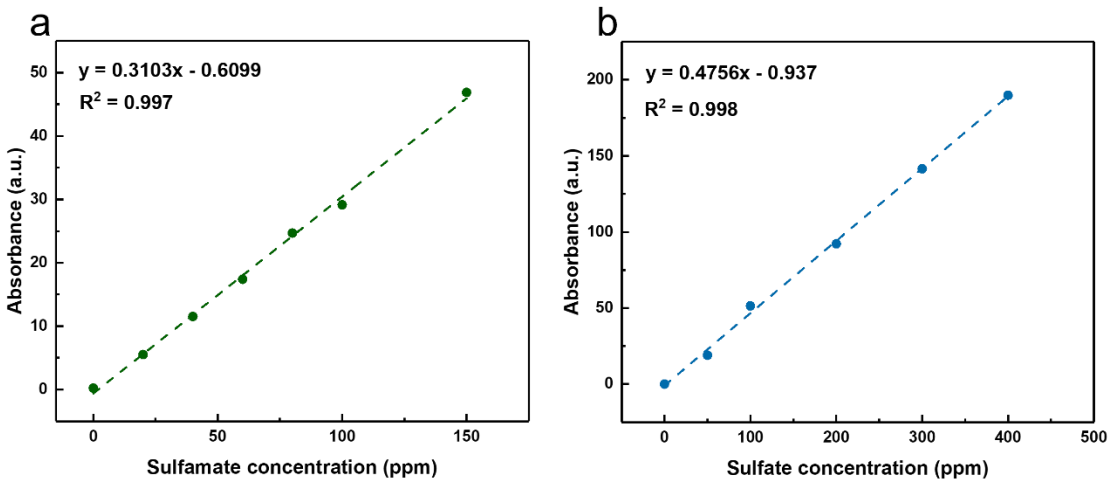

Fig. S15. IC calibration curves of a) sulfamate, and b) sulfate ions using sulfamic acid and sodium sulfate, respectively.

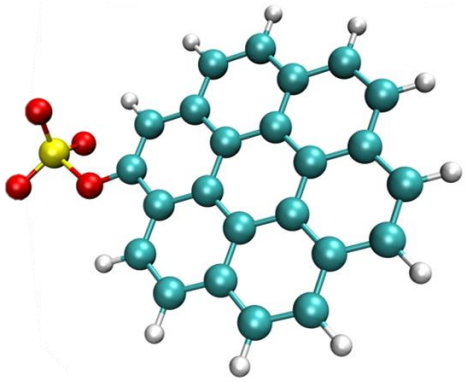

Fig. S16. The adsorption configuration diagram of *SO_3 on the carbon surface.[4,5]

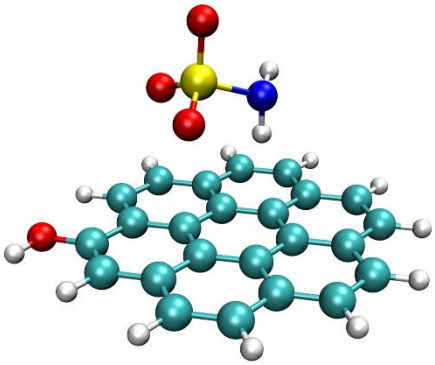

Fig. S17. The configuration diagram of sulfamate product on the carbon surface.[4,5]

Supplementary Table

Table S1. EDS elemental distribution.

Type	Element	Wt%	PTFE wt%
Carbon paper	C	99.58	0
	F	0	
20% PTFE carbon paper	C	74.09	33.9%
	F	25.78	
40% PTFE carbon paper	C	64.74	46.0%
	F	35.00	
60% PTFE carbon paper	C	50.34	65.1%
	F	49.50	

Reference

1 McLean, A. D. & Chandler, G. S. Contracted Gaussian basis sets for molecular calculations. I. Second row atoms, Z=11–18. *The Journal of Chemical Physics* **72**, 5639-5648, (1980).

2 Frisch, M. *et al.* Gaussian 16, Gaussian 16 Revision C. 01. *Gaussian Inc., Wallingford, CT*, (2016).

3 Raghavachari, K. Perspective on "Density functional thermochemistry. III. The role of exact exchange". *Theoretical Chemistry Accounts* **103**, 361-363, (2000).

4 Lu, T. & Chen, F. Multiwfn: A multifunctional wavefunction analyzer. *Journal of Computational Chemistry* **33**, 580-592, (2012).

5 Lu, T. A comprehensive electron wavefunction analysis toolbox for chemists, Multiwfn. *The Journal of Chemical Physics* **161**, (2024).